
Informative Features for Model Comparison

Wittawat Jitkrittum

Max Planck Institute for Intelligent Systems
wittawat@tuebingen.mpg.de

Heishiro Kanagawa

Gatsby Unit, UCL
heishirok@gatsby.ucl.ac.uk

Patsorn Sangkloy

Georgia Institute of Technology
patsorn_sangkloy@gatech.edu

James Hays

Georgia Institute of Technology
hays@gatech.edu

Bernhard Schölkopf

Max Planck Institute for Intelligent Systems
bernhard.schoelkopf@tuebingen.mpg.de

Arthur Gretton*

Gatsby Unit, UCL
arthur.gretton@gmail.com

Abstract

Given two candidate models, and a set of target observations, we address the problem of measuring the relative goodness of fit of the two models. We propose two new statistical tests which are nonparametric, computationally efficient (runtime complexity is linear in the sample size), and interpretable. As a unique advantage, our tests can produce a set of examples (informative features) indicating the regions in the data domain where one model fits significantly better than the other. In a real-world problem of comparing GAN models, the test power of our new test matches that of the state-of-the-art test of relative goodness of fit, while being one order of magnitude faster.

1 Introduction

One of the most fruitful areas in recent machine learning research has been the development of effective generative models for very complex and high dimensional data. Chief among these have been the generative adversarial networks [Goodfellow et al., 2014, Arjovsky et al., 2017, Nowozin et al., 2016], where samples may be generated without an explicit generative model or likelihood function. A related thread has emerged in the statistics community with the advent of Approximate Bayesian Computation, where simulation-based models without closed-form likelihoods are widely applied in bioinformatics applications [see Lintusaari et al., 2017, for a review]. In these cases, we might have several competing models, and wish to evaluate which is the better fit for the data.

The problem of model criticism is traditionally defined as follows: how well does a model Q fit a given sample $Z_n := \{z_i\}_{i=1}^n \stackrel{i.i.d.}{\sim} R$? This task can be addressed in two ways: by comparing samples $Y_n := \{y_i\}_{i=1}^n$ from the model Q and data samples, or by directly evaluating the goodness of fit of the model itself. In both of these cases, the tests have a null hypothesis (that the model agrees with the data), which they will reject given sufficient evidence. Two-sample tests fall into the first category: there are numerous nonparametric tests which may be used [Alba Fernández et al., 2008, Gretton et al., 2012a, Friedman and Rafsky, 1979, Székely and Rizzo, 2004, Rosenbaum, 2005, Harchaoui et al., 2008, Hall and Tajvidi, 2002, Jitkrittum et al., 2016], and recent work in applying two-sample tests to the problem of model criticism [Lloyd and Ghahramani, 2015]. A second approach requires the model density q explicitly. In the case of simple models for which normalisation is not an issue (e.g., checking for Gaussianity), several tests exist [Baringhaus and Henze, 1988, Székely and Rizzo,

*Arthur Gretton's ORCID ID: 0000-0003-3169-7624.

2005]; when a model density is known only up to a normalisation constant, tests of goodness of fit have been developed using a Stein-based divergence [Chwialkowski et al., 2016, Liu et al., 2016, Jitkrittum et al., 2017b].

An issue with the above notion of model criticism, particularly in the case of modern generative models, is that *any* hypothetical model Q that we design is likely a poor fit to the data. Indeed, as noted in Yamada et al. [2018, Section 5.5], comparing samples from various Generative Adversarial Network (GAN) models [Goodfellow et al., 2014] to the reference sample Z_n by a variant of the Maximum Mean Discrepancy (MMD) test [Gretton et al., 2012a] leads to the trivial conclusion that all models are wrong [Box, 1976], i.e., $H_0: Q = R$ is rejected by the test in all cases. A more relevant question in practice is thus: “Given two models P and Q , which is closer to R , and in what ways?” This is the problem we tackle in this work.

To our knowledge, the only nonparametric statistical test of *relative* goodness of fit is the Rel-MMD test of Bounliphone et al. [2015], based on the maximum mean discrepancy [MMD, Gretton et al., 2012a]. While shown to be practical (e.g., for comparing network architectures of generative networks), two issues remain to be addressed. Firstly, its runtime complexity is quadratic in the sample size n , meaning that it can be applied only to problems of moderate size. Secondly and more importantly, it does not give an indication of where one model is better than the other. This is essential for model comparison: in practical settings, it is highly unlikely that one model will be uniformly better than another in all respects: for instance, in hand-written digit generation, one model might produce better “3”s, and the other better “6”s. The ability to produce a few examples which indicate regions (in the data domain) in which one model fits better than the other will be a valuable tool for model comparison. This type of interpretability is useful especially in learning generative models with GANs, where the “mode collapse” problem is widespread [Salimans et al., 2016, Srivastava et al., 2017]. The idea of generating such distinguishing examples (so called *test locations*) was explored in Jitkrittum et al. [2016, 2017b] in the context of model criticism and two-sample testing.

In this work, we propose two new linear-time tests for relative goodness-of-fit. In the first test, the two models P, Q are represented by their two respective samples X_n and Y_n , and the test generalises that of Jitkrittum et al. [2016]. In the second, the test has access to the probability density functions p, q of the two respective candidate models P, Q (which need only be known up to normalisation), and is a three-way analogue of the test of Jitkrittum et al. [2017b]. In both cases, the tests return locations indicating where one model outperforms the other. We emphasise that the practitioner must choose the model ordering, since as noted earlier, this will determine the locations that the test prioritises. We further note that the two tests complement each other, as both address different aspects of the model comparison problem. The first test simply finds the location where the better model produces mass closest to the test sample: a worse model can produce too much mass, or too little. The second test does not address the overall probability mass, but rather the shape of the model density: specifically, it penalises the model whose derivative log density differs most from the target (the interpretation is illustrated in our experiments). In the experiment on comparing two GAN models, we find that the performance of our new test matches that of Rel-MMD while being one order of magnitude faster. Further, unlike the popular Fréchet Inception Distance (FID) [Heusel et al., 2017] which can give a wrong conclusion when two GANs have equal goodness of fit, our proposed method has a well-calibrated threshold, allowing the user to flexibly control the false positive rate.

2 Measures of Goodness of Fit

In the proposed tests, we test the relative goodness of fit by comparing the relative magnitudes of two distances, following Bounliphone et al. [2015]. More specifically, let $D(P, R)$ be a discrepancy measure between P and R . Then, the problem can be formulated as a hypothesis test proposing $H_0: D(P, R) \leq D(Q, R)$ against $H_1: D(P, R) > D(Q, R)$. This is the approach taken by Bounliphone et al. who use the MMD as D , resulting in the relative MMD test (Rel-MMD). The proposed Rel-UME and Rel-FSSD tests are based on two recently proposed discrepancy measures for D : the Unnormalized Mean Embeddings (UME) statistic [Chwialkowski et al., 2015, Jitkrittum et al., 2016], and the Finite-Set Stein Discrepancy (FSSD) [Jitkrittum et al., 2017b], for the sample-based and density-based settings, respectively. We first review UME and FSSD. We will extend these two measures to construct two new relative goodness-of-fit tests in Section 3. We assume throughout that the probability measures P, Q, R have a common support $\mathcal{X} \subseteq \mathbb{R}^d$.

The Unnormalized Mean Embeddings (UME) Statistic UME is a (random) distance between two probability distributions [Chwialkowski et al., 2015] originally proposed for two-sample testing for

$H_0: Q = R$ and $H_1: Q \neq R$. Let $k_Y: \mathcal{X} \times \mathcal{X} \rightarrow \mathbb{R}$ be a positive definite kernel. Let μ_Q be the mean embedding of Q , and is defined such that $\mu_Q(\mathbf{w}) := \mathbb{E}_{\mathbf{y} \sim Q} k(\mathbf{y}, \mathbf{w})$ (assumed to exist) [Smola et al., 2007]. Gretton et al. [2012a] shows that when k_Y is characteristic [Sriperumbudur et al., 2011], the Maximum Mean Discrepancy (MMD) *witness function* $\text{wit}_{Q,R}(\mathbf{w}) := \mu_Q(\mathbf{w}) - \mu_R(\mathbf{w})$ is a zero function if and only if $Q = R$. Based on this fact, the UME statistic evaluates the squared witness function at J_q test locations $W := \{\mathbf{w}_j\}_{j=1}^{J_q} \subset \mathcal{X}$ to determine whether it is zero. Formally, the population squared UME statistic is defined as $U^2(Q, R) := \frac{1}{J} \sum_{j=1}^{J_q} (\mu_Q(\mathbf{w}_j) - \mu_R(\mathbf{w}_j))^2$. For our purpose, it will be useful to rewrite the UME statistic as follows. Define the feature function $\psi_W(\mathbf{y}) := \frac{1}{\sqrt{J_q}} (k_Y(\mathbf{y}, \mathbf{w}_1), \dots, k_Y(\mathbf{y}, \mathbf{w}_{J_q}))^\top \in \mathbb{R}^{J_q}$. Let $\psi_W^Q := \mathbb{E}_{\mathbf{y} \sim Q} [\psi_W(\mathbf{y})]$, and its empirical estimate $\hat{\psi}_W^Q := \frac{1}{n} \sum_{i=1}^n \psi_W(\mathbf{y}_i)$. The squared population UME statistic is equivalent to $U^2(Q, R) := \|\psi_W^Q - \psi_W^R\|_2^2$. For $W \sim \eta$ where η is a distribution with a density, Theorem 2 in Chwialkowski et al. [2015] states that if k_Y is real analytic, integrable, and characteristic, then η -almost surely $\|\psi_W^Q - \psi_W^R\|_2^2 = 0$ if and only if $Q = R$. In words, under the stated conditions, $U(Q, R) := U_Q$ defines a distance between Q and R (almost surely).² A consistent unbiased estimator is $\widehat{U}_Q^2 = \frac{1}{n(n-1)} [\|\sum_{i=1}^n [\psi_W(\mathbf{y}_i) - \psi_W(\mathbf{z}_i)]\|^2 - \sum_{i=1}^n \|\psi_W(\mathbf{y}_i) - \psi_W(\mathbf{z}_i)\|^2]$, which clearly can be computed in $\mathcal{O}(n)$ time. Jitkrittum et al. [2016] proposed optimizing the test locations W and k_Y so as to maximize the test power (i.e., the probability of rejecting H_0 when it is false) of the two-sample test with the normalized version of the UME statistic. It was shown that the optimized locations give an interpretable indication of where Q and R differ in the input domain \mathcal{X} .

The Finite-Set Stein Discrepancy (FSSD) FSSD is a discrepancy between two density functions q and r . Let $\mathcal{X} \subseteq \mathbb{R}^d$ be a connected open set. Assume that Q, R have probability density functions denoted by q, r respectively. Given a positive definite kernel k_Y , the *Stein witness function* [Chwialkowski et al., 2016, Liu et al., 2016] $\mathbf{g}^{q,r}: \mathcal{X} \rightarrow \mathbb{R}^d$ between q and r is defined as $\mathbf{g}^{q,r}(\mathbf{w}) := \mathbb{E}_{\mathbf{z} \sim r} [\boldsymbol{\xi}^q(\mathbf{z}, \mathbf{w})] = (g_1^{q,r}(\mathbf{w}), \dots, g_d^{q,r}(\mathbf{w}))^\top$, where $\boldsymbol{\xi}^q(\mathbf{z}, \mathbf{w}) := k_Y(\mathbf{z}, \mathbf{w}) \nabla_{\mathbf{z}} \log q(\mathbf{z}) + \nabla_{\mathbf{z}} k_Y(\mathbf{z}, \mathbf{w})$. Under appropriate conditions (see Chwialkowski et al. [2016, Theorem 2.2] and Liu et al. [2016, Proposition 3.3]), it can be shown that $\mathbf{g}^{q,r} = \mathbf{0}$ (i.e., the zero function) if and only if $q = r$. An implication of this result is that the deviation of $\mathbf{g}^{q,r}$ from the zero function can be used as a measure of mismatch between q and r . Different ways to characterize such deviation have led to different measures of goodness of fit.

The FSSD characterizes such deviation from $\mathbf{0}$ by evaluating $\mathbf{g}^{q,r}$ at J_q test locations. Formally, given a set of test locations $W = \{\mathbf{w}_j\}_{j=1}^{J_q}$, the squared FSSD is defined as $\text{FSSD}_q^2(r) := \frac{1}{dJ_q} \sum_{j=1}^{J_q} \|\mathbf{g}^{q,r}(\mathbf{w}_j)\|_2^2 := F_q^2$ [Jitkrittum et al., 2017b]. Under appropriate conditions, it is known that almost surely $F_q^2 = 0$ if and only if $q = r$. Using the notations as in Jitkrittum et al. [2017b], one can write $F_q^2 = \mathbb{E}_{\mathbf{z} \sim r} \mathbb{E}_{\mathbf{z}' \sim r} \Delta_q(\mathbf{z}, \mathbf{z}')$ where $\Delta_q(\mathbf{z}, \mathbf{z}') := \boldsymbol{\tau}_q^\top(\mathbf{z}) \boldsymbol{\tau}_q(\mathbf{z}')$, $\boldsymbol{\tau}_q(\mathbf{z}) := \text{vec}(\boldsymbol{\Xi}^q(\mathbf{z})) \in \mathbb{R}^{dJ_q}$, $\text{vec}(\mathbf{M})$ concatenates columns of \mathbf{M} into a column vector, and $\boldsymbol{\Xi}^q(\mathbf{z}) \in \mathbb{R}^{d \times J_q}$ is defined such that $[\boldsymbol{\Xi}^q(\mathbf{z})]_{i,j} := \xi_i^q(\mathbf{z}, \mathbf{w}_j) / \sqrt{dJ_q}$ for $i = 1, \dots, d$ and $j = 1, \dots, J_q$. Equivalently, $F_q^2 = \|\boldsymbol{\mu}_q\|_2^2$ where $\boldsymbol{\mu}_q := \mathbb{E}_{\mathbf{z} \sim r} [\boldsymbol{\tau}_q(\mathbf{z})]$. Similar to the UME statistic described previously, given a sample $Z_n = \{\mathbf{z}_i\}_{i=1}^n \sim r$, an unbiased estimator of F_q^2 , denoted by \widehat{F}_q^2 can be straightforwardly written as a second-order U-statistic, which can be computed in $\mathcal{O}(J_q n)$ time. It was shown in Jitkrittum et al. [2017b] that the test locations W can be chosen by maximizing the test power of the goodness-of-fit test proposing $H_0: q = r$ against $H_1: q \neq r$, using \widehat{F}_q^2 as the statistic. We note that, unlike UME, \widehat{F}_q^2 requires access to the density q . Another way to characterize the deviation of $\mathbf{g}^{q,r}$ from the zero function is to use the norm in the reproducing kernel Hilbert space (RKHS) that contains $\mathbf{g}^{q,r}$. This measure is known as the Kernel Stein Discrepancy having a runtime complexity of $\mathcal{O}(n^2)$ [Chwialkowski et al., 2016, Liu et al., 2016, Gorham and Mackey, 2015].

3 Proposal: Rel-UME and Rel-FSSD Tests

Relative UME (Rel-UME) Our first proposed relative goodness-of-fit test based on UME tests $H_0: U^2(P, R) \leq U^2(Q, R)$ versus $H_1: U^2(P, R) > U^2(Q, R)$. The test uses $\sqrt{n} \widehat{S}_n^U = \sqrt{n} (\widehat{U}_P^2 -$

²In this work, since the distance is always measured relative to the data generating distribution R , we write U_Q instead of $U(Q, R)$ to avoid cluttering the notation.

\widehat{U}_Q^2) as the statistic, and rejects H_0 when it is larger than the threshold T_α . The threshold is given by the $(1 - \alpha)$ -quantile of the asymptotic distribution of $\sqrt{n}\widehat{S}_n^U$ when H_0 holds i.e., the null distribution, and the pre-chosen α is the significance level. It is well-known that this choice for the threshold asymptotically controls the false rejection rate to be bounded above by α yielding a level- α test [Casella and Berger, 2002, Definition 8.3.6]. In the full generality of Rel-UME, two sets of test locations can be used: $V = \{\mathbf{v}_j\}_{j=1}^{J_p}$ for computing \widehat{U}_P^2 , and $W = \{\mathbf{w}_j\}_{j=1}^{J_q}$ for \widehat{U}_Q^2 . The feature function for \widehat{U}_P^2 is denoted by $\psi_V(\mathbf{x}) := \frac{1}{\sqrt{J_p}} (k_X(\mathbf{x}, \mathbf{v}_1), \dots, k_X(\mathbf{x}, \mathbf{v}_{J_p}))^\top \in \mathbb{R}^{J_p}$, for some kernel k_X which can be different from k_Y used in ψ_W . The asymptotic distribution of the statistic is stated in Theorem 1.

Theorem 1 (Asymptotic distribution of \widehat{S}_n^U). *Define $C_W^Q := \text{cov}_{\mathbf{y} \sim Q}[\psi_W(\mathbf{y}), \psi_W(\mathbf{y})]$, $C_V^P := \text{cov}_{\mathbf{x} \sim P}[\psi_V(\mathbf{x}), \psi_V(\mathbf{x})]$, and $C_{VW}^R := \text{cov}_{\mathbf{z} \sim R}[\psi_V(\mathbf{z}), \psi_W(\mathbf{z})] \in \mathbb{R}^{J_p \times J_q}$. Let $S^U := U_P^2 - U_Q^2$, and $\mathbf{M} := \begin{pmatrix} \psi_V^P - \psi_V^R & \mathbf{0} \\ \mathbf{0} & \psi_W^Q - \psi_W^R \end{pmatrix} \in \mathbb{R}^{(J_p + J_q) \times 2}$. Assume that 1) P, Q and R are all distinct, 2) (k_X, V) are chosen such that $U_P^2 > 0$, and (k_Y, W) are chosen such that $U_Q^2 > 0$, 3) $\begin{pmatrix} \zeta_P^2 & \zeta_{PQ} \\ \zeta_{PQ} & \zeta_Q^2 \end{pmatrix} := \mathbf{M}^\top \begin{pmatrix} C_V^P + C_{VW}^R & C_{VW}^R \\ (C_{VW}^R)^\top & C_W^Q + C_W^R \end{pmatrix} \mathbf{M}$ is positive definite. Then, $\sqrt{n}(\widehat{S}_n^U - S^U) \xrightarrow{d} \mathcal{N}(0, 4(\zeta_P^2 - 2\zeta_{PQ} + \zeta_Q^2))$*

A proof of Theorem 1 can be found in Section C.1 (appendix). Let $\nu := 4(\zeta_P^2 - 2\zeta_{PQ} + \zeta_Q^2)$. Theorem 1 states that the asymptotic distribution of \widehat{S}_n^U is normal with the mean given by $S^U := U_P^2 - U_Q^2$. It follows that under H_0 , $S^U \leq 0$ and the $(1 - \alpha)$ -quantile is $S^U + \sqrt{\nu}\Phi^{-1}(1 - \alpha)$ where Φ^{-1} is the quantile function of the standard normal distribution. Since S^U is unknown in practice, we therefore adjust it to be $\sqrt{\nu}\Phi^{-1}(1 - \alpha)$, and use it as the test threshold T_α . The adjusted threshold can be estimated easily by replacing ν with $\hat{\nu}_n$, a consistent estimate based on samples. It can be shown that the test with the adjusted threshold is still level- α (more conservative in rejecting H_0). We note that the same approach of adjusting the threshold is used in Rel-MMD [Bounliphone et al., 2015].

Better Fit of Q in Terms of W . When specifying V and W , the model comparison is done by comparing the goodness of fit of P (to R) as measured in the regions specified by V to the goodness of fit of Q as measured in the regions specified by W . By specifying V and setting $W = V$, testing with Rel-UME is equivalent to posing the question “Does Q fit to the data better than P does, as measured in the regions of V ?” For instance, the observed sample from R might contain smiling and non-smiling faces, and P, Q are candidate generative models for face images. If we are interested in checking the relative fit in the regions of smiling faces, V can be a set of smiling faces. In the followings, we will assume $V = W$ and $k := k_X = k_Y$ for interpretability. Investigating the general case without these constraints will be an interesting topic of future study. Importantly we emphasize that test results are always conditioned on the specified V . To be precise, let U_V^2 be the squared UME statistic defined by V . It is entirely realistic that the test rejects H_0 in favor of $H_1 : U_{V_1}^2(P, R) > U_{V_1}^2(Q, R)$ (i.e., Q fits better) for some V_1 , and also rejects H_0 in favor of the opposite alternative $H_1 : U_{V_2}^2(Q, R) > U_{V_2}^2(P, R)$ (i.e., P fits better) for another setting of V_2 . This is because the regions in which the model comparison takes place are different in the two cases. Although not discussed in Bounliphone et al. [2015], the same behaviour can be observed for Rel-MMD i.e., test results are conditioned on the choice of kernel.

In some cases, it is not known in advance what features are better represented by one model vs another, and it becomes necessary to learn these features from the model outputs. In this case, we propose setting V to contain the locations which maximize the probability that the test can detect the better fit of Q , as measured at the locations. Following the same principle as in Gretton et al. [2012b], Sutherland et al. [2016], Jitkrittum et al. [2016, 2017a,b], this goal can be achieved by finding (k, V) which maximize the test power, while ensuring that the test is level- α . By Theorem 1, for large n the test power $\mathbb{P}(\sqrt{n}\widehat{S}_n^U > T_\alpha)$ is approximately $\Phi\left(\frac{\sqrt{n}S^U - T_\alpha}{\sqrt{\nu}}\right) = \Phi\left(\sqrt{n}\frac{S^U}{\sqrt{\nu}} - \sqrt{\frac{\hat{\nu}_n}{\nu}}\Phi^{-1}(1 - \alpha)\right)$. Under H_1 , $S^U > 0$. For large n , $\Phi^{-1}(1 - \alpha)\sqrt{\hat{\nu}_n}/\sqrt{\nu}$ approaches a constant, and $\sqrt{n}S^U/\sqrt{\nu}$ dominates. It follows that, for large n , $(k^*, V^*) = \arg \max_{(k, V)} \mathbb{P}(\sqrt{n}\widehat{S}_n^U > T_\alpha) \approx \arg \max_{(k, V)} S^U/\sqrt{\nu}$. We

can thus use $\hat{S}_n^U / (\gamma + \sqrt{\hat{v}_n})$ as an estimate of the *power criterion* objective S^U / \sqrt{v} for the test power, where $\gamma > 0$ is a small regularization parameter added to promote numerical stability following Jitkrittum et al. [2017b, p. 5]. To control the false rejection rate, the maximization is carried out on held-out training data which are independent of the data used for testing. In the experiments (Section 4), we hold out 20% of the data for the optimization. A unique consequence of this procedure is that we obtain optimized V^* which indicates where Q fits significantly better than P . We note that this interpretation only holds if the test, using the optimized hyperparameters (k^*, V^*) , decides to reject H_0 . The optimized locations may not be interpretable if the test fails to reject H_0 .

Relative FSSD (Rel-FSSD) The proposed Rel-FSSD tests $H_0: F_p^2 \leq F_q^2$ versus $H_1: F_p^2 > F_q^2$. The test statistic is $\sqrt{n}\hat{S}_n^F := \sqrt{n}(\widehat{F}_p^2 - \widehat{F}_q^2)$. We note that the feature functions τ_p (for F_p^2) and τ_q (for F_q^2) depend on (k_X, V) and (k_Y, W) respectively, and play the same role as the feature functions ψ_V and ψ_W of the UME statistic. Due to space limitations, we only state the salient facts of Rel-FSSD. The rest of the derivations closely follow Rel-UME. These include the interpretation that the relative fit is measured at the specified locations given in V and W , and the derivation of Rel-FSSD’s power criterion (which can be derived using the asymptotic distribution of \hat{S}_n^F given in Theorem 2, following the same line of reasoning as in the case of Rel-UME). A major difference is that Rel-FSSD requires explicit (gradients of the log) density functions of the two models, allowing it to gain structural information of the models that may not be as easily observed in finite samples. We next state the asymptotic distribution of the statistic (Theorem 2), which is needed for obtaining the threshold and for deriving the power criterion. The proof closely follows the proof of Theorem 1, and is omitted.

Theorem 2 (Asymptotic distribution of \hat{S}_n^F). *Define $S^F := F_p^2 - F_q^2$. Let $\Sigma^{ss'} := \text{cov}_{\mathbf{z} \sim r}[\tau_s(\mathbf{z}), \tau_{s'}(\mathbf{z})]$ for $s, s' \in \{p, q\}$ so that $\Sigma^{pq} \in \mathbb{R}^{dJ_p \times dJ_q}$, $\Sigma^{qp} := (\Sigma^{pq})^\top$, $\Sigma^{pp} = \Sigma^p \in \mathbb{R}^{dJ_p \times dJ_p}$, and $\Sigma^{qq} = \Sigma^q \in \mathbb{R}^{dJ_q \times dJ_q}$. Assume that 1) p, q , and r are all distinct, 2) (k_X, V) are chosen such that $F_p^2 > 0$, and (k_Y, W) are chosen such that $F_q^2 > 0$, 3) $\begin{pmatrix} \sigma_p^2 & \sigma_{pq} \\ \sigma_{pq} & \sigma_q^2 \end{pmatrix} := \begin{pmatrix} \mu_p^\top \Sigma^p \mu_p & \mu_p^\top \Sigma^{pq} \mu_q \\ \mu_p^\top \Sigma^{pq} \mu_q & \mu_q^\top \Sigma^q \mu_q \end{pmatrix}$ is positive definite. Then, $\sqrt{n}(\hat{S}_n^F - S^F) \xrightarrow{d} \mathcal{N}(0, 4(\sigma_p^2 - 2\sigma_{pq} + \sigma_q^2))$.*

4 Experiments

In this section, we demonstrate the two proposed tests on both toy and real problems. We start with an illustration of the behaviors of Rel-UME and Rel-FSSD’s power criteria using simple one-dimensional problems. In the second experiment, we examine the test powers of the two proposed tests using three toy problems. In the third experiment, we compare two hypothetical generative models on the CIFAR-10 dataset [Krizhevsky and Hinton, 2009] and demonstrate that the learned test locations (images) can clearly indicate the types of images that are better modeled by one of the two candidate models. In the last two experiments, we consider the problem of determining the relative goodness of fit of two given Generative Adversarial Networks (GANs) [Goodfellow et al., 2014]. Code to reproduce all the results is available at <https://github.com/wittawatj/kernel-mod>.

1. Illustration of Rel-UME and Rel-FSSD Power Criteria We consider $k = k_X = k_Y$ to be a Gaussian kernel, and set $V = W = \{v\}$ (one test location). The power criterion of Rel-UME as a function of v can be written as $\frac{1}{2} \frac{\text{wit}_{P,R}^2(v) - \text{wit}_{Q,R}^2(v)}{(\zeta_P^2(v) - 2\zeta_{PQ}(v) + \zeta_Q^2(v))^{1/2}}$ where $\text{wit}(\cdot)$ is the MMD witness function (see Section 2), and we explicitly indicate the dependency on v . To illustrate, we consider two Gaussian models p, q with different means but the same variance, and set r to be a mixture of p and q . Figure 1a shows that when each component in r has the same mixing proportion, the power criterion of Rel-UME is a zero function indicating that p and q have the same goodness of fit to r everywhere. To understand this, notice that at the left mode of r , p has excessive probability mass (compared to r), while q has almost no mass at all. Both models are thus wrong at the left mode of r . However, since the extra probability mass of p is equal to the missing mass of q , Rel-UME considers p and q as having the same goodness of fit. In Figure 1b, the left mode of r now has a mixing proportion of only 30%, and r more closely matches q . The power criterion is thus positive at the left mode indicating that q has a better fit.

The power criterion of Rel-FSSD indicates that q fits better at the right mode of r in the case of equal mixing proportion (see Figure 1c). In one dimension, the Stein witness function $\mathbf{g}^{q,r}$ (defined

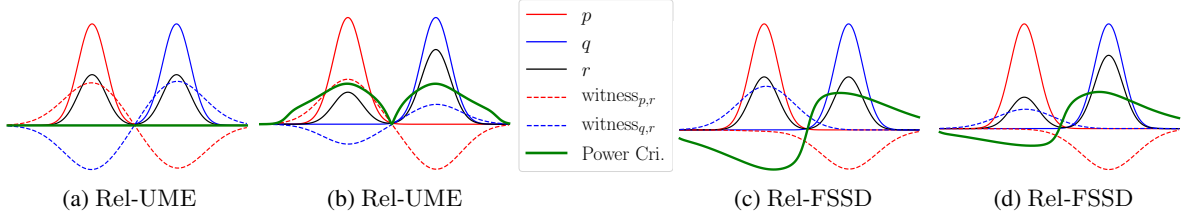


Figure 1: One-dimensional plots (in green) of Rel-UME’s power criteria (in (a), (b)), and Rel-FSSD’s power criteria (in (c), (d)). The dashed lines in (a), (b) indicate MMD’s witness functions used in Rel-UME, and the dashed lines in (c), (d) indicate FSSD’s Stein witness functions.

in Section 2) can be written as $g^{q,r}(w) = \mathbb{E}_{z \sim r} [k_Y(z, w) \nabla_z (\log q(z) - \log r(z))]$, which is the expectation under r of the difference in the derivative log of q and r , weighted by the kernel k_Y . The Stein witness thus only captures the matching of the shapes of the two densities (as given by the derivative log). Unlike the MMD witness, the Stein witness is insensitive to the mismatch of probability masses i.e., it is independent of the normalizer of q . In Figure 1c, since the shape of q and the shape of the right mode of r match, the Stein witness $g^{q,r}$ (dashed blue curve) vanishes at the right mode of r , indicating a good fit of q in the region. The mismatch between the shape of q and the shape of r at the left mode of r is what creates the peak of $g^{q,r}$. The same reasoning holds for the Stein witness $g^{p,r}$. The power criterion of Rel-FSSD, which is given by $\frac{1}{2} \frac{g^{p,r}(w)^2 - g^{q,r}(w)^2}{(\sigma_p^2(w) - 2\sigma_{pq}(w) + \sigma_q^2(w))^{1/2}}$, is thus positive at the right mode of r (shapes of q and r matched there), and negative at the left mode of r (shapes of p and r matched there). To summarize, Rel-UME measures the relative fit by checking the probability mass, while Rel-FSSD does so by matching the shapes of the densities.

2. Test Powers on Toy Problems The goal of this experiment is to investigate the rejection rates of several variations of the two proposed tests. To this end, we study three toy problems, each having its own characteristics. All the three distributions in each problem have density functions to allow comparison with Rel-FSSD.

1. *Mean shift*: All the three distributions are isotropic multivariate normal distributions: $p = \mathcal{N}([0.5, 0, \dots, 0], \mathbf{I})$, $q = \mathcal{N}([1, 0, \dots, 0], \mathbf{I})$, and $r = \mathcal{N}(\mathbf{0}, \mathbf{I})$, defined on \mathbb{R}^{50} . The two candidates models p and q differ in the mean of the first dimension. In this problem, the null hypothesis H_0 is true since p is closer to r .
2. *Blobs*: Each distribution is given by a mixture of four Gaussian distributions organized in a grid in \mathbb{R}^2 . Samples from p , q and r are shown in Figure 4. In this problem, q is closer to r than p is i.e., H_1 is true. One characteristic of this problem is that the difference between p and q takes place in a small scale relative to the global structure of the data. This problem was studied in Gretton et al. [2012b], Chwialkowski et al. [2015].
3. *RBM*: Each of the three distributions is given by a Gaussian Bernoulli Restricted Boltzmann Machine (RBM) model with density function $p'_{\mathbf{B}, \mathbf{b}, \mathbf{c}}(\mathbf{x}) = \sum_{\mathbf{h}} p'_{\mathbf{B}, \mathbf{b}, \mathbf{c}}(\mathbf{x}, \mathbf{h})$, where $p'_{\mathbf{B}, \mathbf{b}, \mathbf{c}}(\mathbf{x}, \mathbf{h}) := \frac{1}{Z} \exp\left(\mathbf{x}^\top \mathbf{B} \mathbf{h} + \mathbf{b}^\top \mathbf{x} + \mathbf{c}^\top \mathbf{h} - \frac{1}{2} \|\mathbf{x}\|^2\right)$, $\mathbf{h} \in \{-1, 1\}^{d_h}$ is a latent vector, Z is the normalizer, and $\mathbf{B}, \mathbf{b}, \mathbf{c}$ are model parameters. Let $r(\mathbf{x}) := p'_{\mathbf{B}, \mathbf{b}, \mathbf{c}}(\mathbf{x})$, $p(\mathbf{x}) := p'_{\mathbf{B}^p, \mathbf{b}, \mathbf{c}}(\mathbf{x})$, and $q(\mathbf{x}) := p'_{\mathbf{B}^q, \mathbf{b}, \mathbf{c}}(\mathbf{x})$. Following a similar setting as in Liu et al. [2016], Jitkritum et al. [2017b], we set the parameters of the data generating density r by uniformly randomly setting entries of \mathbf{B} to be from $\{-1, 1\}$, and drawing entries of \mathbf{b} and \mathbf{c} from the standard normal distribution. Let δ be a matrix of the same size as \mathbf{B} such that $\delta_{1,1} = 1$ and all other entries are 0. We set $\mathbf{B}^q = \mathbf{B} + 0.3\delta$ and $\mathbf{B}^p = \mathbf{B} + \epsilon\delta$, where the perturbation constant ϵ is varied. We fix the sample size n to 2000. Perturbing only one entry of \mathbf{B} creates a problem in which the difference of distributions can be difficult to detect. This serves as a challenging benchmark to measure the sensitivity of statistical tests [Jitkritum et al., 2017b]. We set $d = 20$ and $d_h = 5$.

We compare three kernel-based tests: Rel-UME, Rel-FSSD, and Rel-MMD (the relative MMD test of Bounliphone et al. [2015]), all using a Gaussian kernel. For Rel-UME and Rel-FSSD we set $k_X = k_Y = k$, where the the Gaussian width of k , and the test locations are chosen by maximizing their respective power criteria described in Section 3 on 20% of the data. The optimization procedure is described in Section A (appendix). Following Bounliphone et al. [2015], the Gaussian width of Rel-MMD is chosen by the median heuristic as implemented in the code by the authors. In the RBM

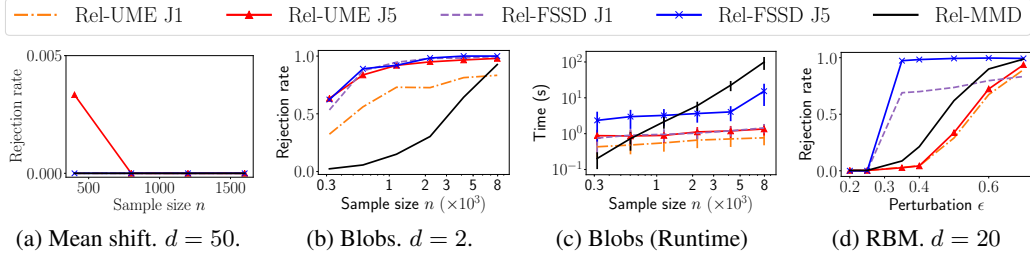


Figure 2: (a), (b), (d) Rejection rates (estimated from 300 trials) of the five tests with $\alpha = 0.05$. In the RBM problem, $n = 2000$. (c) Runtime in seconds for one trial in the Blobs problem.

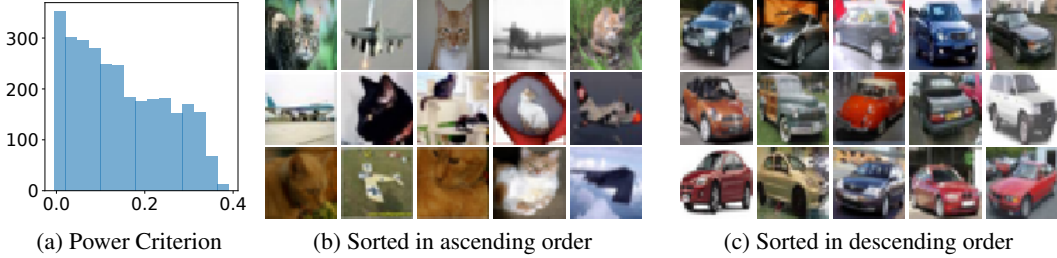


Figure 3: $P = \{\text{airplane, cat}\}$, $Q = \{\text{automobile, cat}\}$, and $R = \{\text{automobile, cat}\}$. (a) Histogram of Rel-UME power criterion values. (b), (c) Images as sorted by the criterion values in ascending and descending orders, respectively.

problem, all problem parameters B , b , and c are drawn only once and fixed. Only the samples vary across trials.

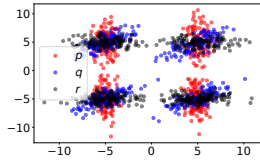


Figure 4: Blobs problem samples: p , q , r .

Figure 2 shows the test powers of all the tests. When H_0 holds, all tests have false rejection rates (type-I errors) bounded above by $\alpha = 0.05$ (Figure 2a). In the Blobs problem (Figure 2b), it can be seen that Rel-UME achieves larger power at all sample sizes, compared to Rel-MMD. Since the relative goodness of fit of p and q must be compared locally, the optimized test locations of Rel-UME are suitable for detecting such local differences. The poor performance of Rel-MMD is caused by unsuitable choices of the kernel bandwidth. The bandwidth chosen by the median heuristic is only appropriate for capturing the global length scale of the problem. It is thus too large to capture small-scale differences. No existing work has proposed a kernel selection procedure for Rel-MMD. Regarding the number J of test locations, we observe that changing J from 1 to 5 drastically increases the test power of Rel-UME, since more regions characterizing the differences can be pinpointed. Rel-MMD exhibits a quadratic-time profile (Figure 2c) as a function of n .

Figure 2d shows the rejection rates against the perturbation strength ϵ in p in the RBM problem. When $\epsilon \leq 0.3$, p is closer to r than q is (i.e., H_0 holds). We observe that all the tests have well-controlled false rejection rates in this case. At $\epsilon = 0.35$, while q is closer (i.e., H_1 holds), the relative amount by which q is closer to r is so small that a significant difference cannot be detected when p and q are represented by samples of size $n = 2000$, hence the low powers of Rel-UME and Rel-MMD. Structural information provided by the density functions allows Rel-FSSD (both $J = 1$ and $J = 5$) to detect the difference even at $\epsilon = 0.35$, as can be seen from the high test powers. The fact that Rel-MMD has higher power than Rel-UME, and the fact that changing J from 1 to 5 increases the power only slightly suggest that the differences may be spatially diffuse (rather than local).

3. Informative Power Objective In this part, we demonstrate that test locations having positive (negative) values of the power criterion correctly indicate the regions in which Q has a better (worse) fit. We consider image samples from three categories of the CIFAR-10 dataset [Krizhevsky and Hinton, 2009]: airplane, automobile, and cat. We partition the images, and assume that the sample from P consists of 2000 airplane, 1500 cat images, the sample from Q consists of 2000 automobile, 1500 cat images, and the reference sample from R consists of 2000 automobile, 1500 cat images. All samples are independent. We consider a held-out random sample consisting of 1000 images from each

Table 1: Rejection rates of the proposed Rel-UME, Rel-MMD, KID and FID, in the GAN model comparison problem. “FID diff.” refers to the average of $FID(P, R) - FID(Q, R)$ estimated in each trial. Significance level $\alpha = 0.01$ (for Rel-UME, Rel-MMD, and KID).

	P	Q	R	Rel-UME			Rel-MMD	KID	FID	FID diff.
				J10	J20	J40				
1.	S	S	RS	0.0	0.0	0.0	0.0	0.0	0.53	-0.045 ± 0.52
2.	RS	RS	RS	0.0	0.0	0.0	0.03	0.02	0.7	0.04 ± 0.19
3.	S	N	RS	0.0	0.0	0.0	0.0	0.0	0.0	-15.22 ± 0.83
4.	S	N	RN	0.57	0.97	1.0	1.0	1.0	1.0	5.25 ± 0.75
5.	S	N	RM	0.0	0.0	0.0	0.0	0.0	0.0	-4.55 ± 0.82

category, serving as a pool of test location candidates. We set the kernel to be the Gaussian kernel on 2048 features extracted by the Inception-v3 network at the pool3 layer [Szegedy et al., 2016]. We evaluate the power criterion of Rel-UME at each of the test locations in the pool individually. The histogram of the criterion values is shown in Figure 3a. We observe that all the power criterion values are non-negative, confirming that Q is better than P everywhere. Figure 3b shows the top 15 test locations as sorted in ascending order by the criterion, consisting of automobile images. These indicate the regions in the data domain where Q fits better. Notice that cat images do not have high positive criterion values because they can be modeled equally well by P and Q , and thus have scores close to zero as shown in Figure 3b.

4. Testing GAN Models In this experiment, we apply the proposed Rel-UME test to comparing two generative adversarial networks (GANs) [Goodfellow et al., 2014]. We consider the CelebA dataset [Liu et al., 2015]³ in which each data point is an image of a celebrity with 40 binary attributes annotated e.g., pointy nose, smiling, mustache, etc. We create a partition of the images on the *smiling* attribute, thereby creating two disjoint subsets of *smiling* and *non-smiling* images. A set of 30000 images from each subset is held out for subsequent relative goodness-of-fit testing, and the rest are used for training two GAN models: a model for smiling images, and a model for non-smiling images. Generated samples and details of the trained models can be found in Section B (appendix). The two models are trained once and fixed throughout.

In addition to Rel-MMD, we compare the proposed Rel-UME to Kernel Inception Distance (KID) [Bińkowski et al., 2018], and Fréchet Inception Distance (FID) [Heusel et al., 2017], which are distances between two samples (originally proposed for comparing a sample of generated images, and a reference sample). All images are represented by 2048 features extracted from the Inception-v3 network [Szegedy et al., 2016] at the pool3 layer following Bińkowski et al. [2018]. When adapted for three samples, KID is in fact a variant of Rel-MMD in which a third-order polynomial kernel is used instead of a Gaussian kernel (on top of the pool3 features). Following Bińkowski et al. [2018], we construct a bootstrap estimator for FID (10 subsamples with 1000 points in each). For the proposed Rel-UME, the $J \in \{10, 20, 40\}$ test locations are randomly set to contain $J/2$ smiling images, and $J/2$ non-smiling images drawn from a held-out set of real images. We create problem variations by setting $P, Q, R \in \{S, N, RS, RN, RM\}$ where S denotes generated smiling images (from the trained model), N denotes generated non-smiling images, M denotes an equal mixture of smiling and non-smiling images, and the prefix R indicates that real images are used (as opposed to generated ones). The sample size is $n = 2000$, and each problem variation is repeated for 10 trials for FID (due to its high complexity) and 100 trials for other methods. The rejection rates from all the methods are shown in Table 1. Here, the test result for FID in each trial is considered “reject H_0 ” if $FID(P, R) > FID(Q, R)$. Heusel et al. [2017] did not propose FID as a statistical test. That said, there is a generic way of constructing a relative goodness-of-fit test based on repeated permutation of samples of P and Q to simulate from the null distribution. However, FID requires computing the square root of the feature covariance matrix (2048 x 2048), and is computationally too expensive for permutation testing.

Overall, we observe that the proposed test does at least equally well as existing approaches, in identifying the better model in each case. In problems 1 and 2, P and Q have the same goodness of fit, by design. In these cases, all the tests correctly yield low rejection rates, staying roughly at the design level ($\alpha = 0.01$). Without a properly chosen threshold, the (false) rejection rates of FID fluctuate

³CelebA dataset: <http://mmlab.ie.cuhk.edu.hk/projects/CelebA.html>.

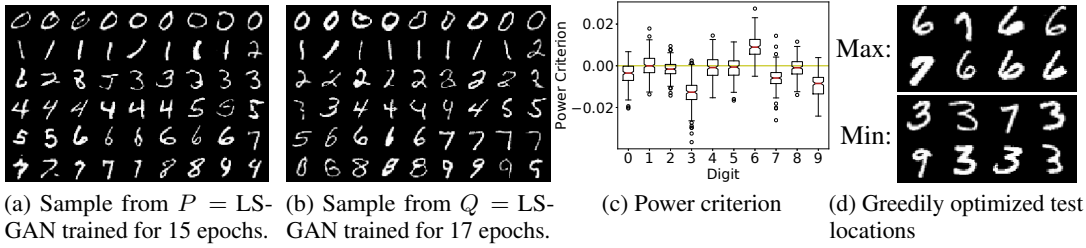


Figure 5: Examining the training of an LSGAN model with Rel-UME. (a), (b) Samples from the two models P, Q trained on MNIST. (c) Distributions of power criterion values computed over 200 trials. Each distribution is formed by randomly selecting $J = 40$ test locations from real images of a digit type. (d) Test locations showing where Q is better (maximization of the power criterion), and test locations showing where P is better (minimization).

around the expected value of 0.5. This means that simply comparing FIDs (or other distances) to the reference sample without a calibrated threshold can lead to a wrong conclusion on the relative goodness of fit. The FID is further complicated by the fact that its estimator suffers from bias in ways that are hard to model and correct for (see Bińkowski et al. [2018, Section D.1]). Problem 4 is a case where the model Q is better. We notice that increasing the number of test locations of Rel-UME helps detect the better fit of Q . In problem 5, the reference sample is bimodal, and each model can capture only one of the two modes (analogous to the synthetic problem in Figure 1a). All the tests correctly indicate that no model is better than another.

5. Examining GAN Training In the final experiment, we show that the power criterion of Rel-UME can be used to examine the relative change of the distribution of a GAN model after training further for a few epochs. To illustrate, we consider training an LSGAN model [Mao et al., 2017] on MNIST, a dataset in which each data point is an image of a handwritten digit. We set P and Q to be LSGAN models after 15 epochs and 17 epochs of training, respectively. Details regarding the network architecture, training, and the kernel (chosen to be a Gaussian kernel on features extracted from a convolutional network) can be found in Section D. Samples from P and Q are shown in Figures 5a and 5b (see Figure 8 in the appendix for more samples).

We set the test locations V to be the set V_i containing $J = 40$ randomly selected real images of digit i , for $i \in \{0, \dots, 9\}$. We then draw $n = 2000$ points from P, Q and the real data (R), and use $V = V_i$ to compute the power criterion for $i \in \{0, \dots, 9\}$. The procedure is repeated for 200 trials where V and the samples are redrawn each time. The results are shown in Figure 5c. We observe that when $V = V_3$ (i.e., box plot at the digit 3) or V_9 , the power criterion values are mostly negative, indicating that P is better than Q , as measured in the regions indicated by real images of the digits 3 or 9. By contrast, when $V = V_6$, the large mass of the box plot in the positive orthant shows that Q is better in the regions of the digit 6. For other digits, the criterion values spread around zero, showing that there is no difference between P and Q , on average. We further confirm that the class proportions of the generated digits from both models are roughly correct (i.e., uniform distribution), meaning that the difference between P and Q in these cases is not due to the mismatch in class proportions (see Section D). These observations imply that after the 15th epoch, training this particular LSGAN model two epochs further improves generation of the digit 6, and degrades generation of digits 3 and 9. A non-monotonic improvement during training is not uncommon since at the 15th epoch the training has not converged. More experimental results from comparing different GAN variants on MNIST can be found in Section E in the appendix.

We note that the set V does not need to contain test locations of the same digit. In fact, the notion of class labels may not even exist in general. It is up to the user to define V to contain examples which capture the relevant concept of interest. For instance, to compare the ability of models to generate straight strokes, one might include digits 1 and 7 in the set V . An alternative to manual specification of V is to optimize the power criterion to find the locations that best distinguish the two models (as done in experiment 2). To illustrate, we consider greedily optimizing the power criterion by iteratively selecting a test location (from real images) which best improves the objective. Maximizing the objective yields locations that indicate the better fit of Q , whereas minimization gives locations which show the better fit of P (recall from Figure 1). The optimized locations are shown in Figure 5d. The results largely agree with our previous observations, and do not require manually specifying V . This optimization procedure is applicable to any models which can be sampled.

Acknowledgments

HK and AG thank the Gatsby Charitable Foundation for the financial support.

References

- V. Alba Fernández, M. Jiménez-Gamero, and J. Muñoz Garcia. A test for the two-sample problem based on empirical characteristic functions. *Computational Statistics and Data Analysis*, 52: 3730–3748, 2008.
- B. Amos, B. Ludwiczuk, and M. Satyanarayanan. Openface: A general-purpose face recognition library with mobile applications. Technical report, CMU-CS-16-118, CMU School of Computer Science, 2016.
- M. Arjovsky, S. Chintala, and L. Bottou. Wasserstein generative adversarial networks. In *ICML*, 2017.
- L. Baringhaus and N. Henze. A consistent test for multivariate normality based on the empirical characteristic function. *Metrika*, 35:339–348, 1988.
- M. Bińkowski, D. J. Sutherland, M. Arbel, and A. Gretton. Demystifying MMD GANs. In *ICLR*, 2018.
- W. Bounliphone, E. Belilovsky, M. B. Blaschko, I. Antonoglou, and A. Gretton. A test of relative similarity for model selection in generative models. In *ICLR*, 2015.
- G. E. P. Box. Science and statistics. *Journal of the American Statistical Association*, 71:791–799, 1976.
- G. Casella and R. L. Berger. *Statistical inference*, volume 2. Duxbury Pacific Grove, CA, 2002.
- X. Chen, Y. Duan, R. Houthoofd, J. Schulman, I. Sutskever, and P. Abbeel. InfoGAN: Interpretable representation learning by information maximizing generative adversarial nets. In *NIPS*, pages 2172–2180, 2016.
- K. Chwialkowski, A. Ramdas, D. Sejdinovic, and A. Gretton. Fast two-sample testing with analytic representations of probability measures. In *NIPS*, pages 1972–1980, 2015.
- K. Chwialkowski, H. Strathmann, and A. Gretton. A kernel test of goodness of fit. In *ICML*, pages 2606–2615, 2016.
- J. Friedman and L. Rafsky. Multivariate generalizations of the Wald-Wolfowitz and Smirnov two-sample tests. *The Annals of Statistics*, 7(4):697–717, 1979.
- I. Goodfellow, J. Pouget-Abadie, M. Mirza, B. Xu, D. Warde-Farley, S. Ozair, A. Courville, and Y. Bengio. Generative adversarial nets. In *NIPS*, pages 2672–2680, 2014.
- J. Gorham and L. Mackey. Measuring sample quality with Stein’s method. In *NIPS*, pages 226–234, 2015.
- A. Gretton, K. Borgwardt, M. Rasch, B. Schölkopf, and A. Smola. A kernel two-sample test. *Journal of Machine Learning Research*, 13:723–773, 2012a.
- A. Gretton, D. Sejdinovic, H. Strathmann, S. Balakrishnan, M. Pontil, K. Fukumizu, and B. K. Sriperumbudur. Optimal kernel choice for large-scale two-sample tests. In *NIPS*, pages 1205–1213, 2012b.
- I. Gulrajani, F. Ahmed, M. Arjovsky, V. Dumoulin, and A. C. Courville. Improved training of Wasserstein GANs. In *NIPS*, pages 5767–5777, 2017.
- P. Hall and N. Tajvidi. Permutation tests for equality of distributions in high-dimensional settings. *Biometrika*, 89(2):359–374, 2002.
- Z. Harchaoui, F. Bach, and E. Moulines. Testing for homogeneity with kernel Fisher discriminant analysis. pages 609–616. MIT Press, Cambridge, MA, 2008.

- M. Heusel, H. Ramsauer, T. Unterthiner, B. Nessler, and S. Hochreiter. GANs trained by a two time-scale update rule converge to a local nash equilibrium. In *NIPS*. 2017.
- W. Hoeffding. A class of statistics with asymptotically normal distribution. *Ann. Math. Statist.*, 19(3):293–325, 09 1948.
- W. Jitkrittum, Z. Szabó, K. P. Chwialkowski, and A. Gretton. Interpretable distribution features with maximum testing power. In *NIPS*, pages 181–189. 2016.
- W. Jitkrittum, Z. Szabó, and A. Gretton. An adaptive test of independence with analytic kernel embeddings. In *ICML*. 2017a.
- W. Jitkrittum, W. Xu, Z. Szabo, K. Fukumizu, and A. Gretton. A linear-time kernel goodness-of-fit test. In *NIPS*, 2017b.
- D. P. Kingma and J. Ba. Adam: A method for stochastic optimization. *ArXiv e-prints*, Dec. 2014.
- A. Krizhevsky and G. Hinton. Learning multiple layers of features from tiny images. 2009.
- J. Lintusaari, M. Gutmann, R. Dutta, S. Kaski, and J. Corander. Fundamentals and recent developments in approximate bayesian computation. *Systematic Biology*, 66(1):e66–e82, 2017.
- Q. Liu, J. Lee, and M. Jordan. A kernelized Stein discrepancy for goodness-of-fit tests. In *ICML*, pages 276–284, 2016.
- Z. Liu, P. Luo, X. Wang, and X. Tang. Deep learning face attributes in the wild. In *Proceedings of International Conference on Computer Vision (ICCV)*, 2015.
- J. R. Lloyd and Z. Ghahramani. Statistical model criticism using kernel two sample tests. In *NIPS*, pages 829–837, 2015.
- X. Mao, Q. Li, H. Xie, R. Y. Lau, Z. Wang, and S. P. Smolley. Least squares generative adversarial networks. In *Computer Vision (ICCV), 2017 IEEE International Conference on*, pages 2813–2821. IEEE, 2017.
- S. Nowozin, B. Cseke, and R. Tomioka. f-GAN: Training generative neural samplers using variational divergence minimization. In *NIPS*, 2016.
- A. Radford, L. Metz, and S. Chintala. Unsupervised representation learning with deep convolutional generative adversarial networks. *arXiv preprint arXiv:1511.06434*, 2015.
- P. Rosenbaum. An exact distribution-free test comparing two multivariate distributions based on adjacency. *Journal of the Royal Statistical Society B*, 67(4):515–530, 2005.
- T. Salimans, I. Goodfellow, W. Zaremba, V. Cheung, A. Radford, and X. Chen. Improved techniques for training GANs. *ArXiv e-prints*, June 2016.
- R. J. Serfling. *Approximation Theorems of Mathematical Statistics*. John Wiley & Sons, 2009.
- A. Smola, A. Gretton, L. Song, and B. Schölkopf. A Hilbert space embedding for distributions. In *International Conference on Algorithmic Learning Theory (ALT)*, pages 13–31, 2007.
- B. K. Sriperumbudur, K. Fukumizu, and G. R. G. Lanckriet. Universality, characteristic kernels and RKHS embedding of measures. *Journal of Machine Learning Research*, 12:2389–2410, 2011.
- A. Srivastava, L. Valkov, C. Russell, M. U. Gutmann, and C. Sutton. VEEGAN: Reducing mode collapse in GANs using implicit variational learning. *ArXiv e-prints*, May 2017.
- D. J. Sutherland, H.-Y. Tung, H. Strathmann, S. De, A. Ramdas, A. Smola, and A. Gretton. Generative models and model criticism via optimized maximum mean discrepancy. In *ICLR*. 2016.
- C. Szegedy, V. Vanhoucke, S. Ioffe, J. Shlens, and Z. Wojna. Rethinking the inception architecture for computer vision. In *Proceedings of the IEEE Conference on Computer Vision and Pattern Recognition*, pages 2818–2826, 2016.
- G. Székely and M. Rizzo. Testing for equal distributions in high dimension. *InterStat*, 5, 2004.

- G. J. Székely and M. L. Rizzo. A new test for multivariate normality. *Journal of Multivariate Analysis*, 93(1):58–80, 2005.
- M. Yamada, D. Wu, Y.-H. H. Tsai, I. Takeuchi, R. Salakhutdinov, and K. Fukumizu. Post selection inference with incomplete maximum mean discrepancy estimator. *arXiv preprint arXiv:1802.06226*, 2018.

Informative Features for Model Comparison

Supplementary

A Optimization of Test Locations in Rel-UME and Rel-FSSD

This section describes the optimization procedure we use to select the test locations V and the bandwidth of the Gaussian kernel in the experiment “Test Powers on Toy Problems.” Since the two sets V, W of test locations are constrained to be the same i.e., $V = W$ consisting of $J = J_p = J_q$ locations, in total, we have $Jd + 1$ parameters. We follow a similar implementation of the optimization procedure for finding the test locations in FSSD.⁴ All the parameters are optimized jointly by gradient ascent. We initialize the test locations by randomly picking J points from the training set. The Gaussian width is initialized (for gradient ascent) to the square of the mean of $\text{med}_{X^{tr} \cup Z^{tr}}$ and $\text{med}_{Y^{tr} \cup Z^{tr}}$, where $\text{med}_A := \text{median}(\{\|\mathbf{x} - \mathbf{x}'\|_2\}_{\mathbf{x}, \mathbf{x}' \in A})$. This is a similar heuristic used in Bounliphone et al. [2015] to set the bandwidth of the Gaussian kernel for Rel-MMD.

B Trained Models for Generating Smiling and Non-Smiling Images



Figure 6: Samples from the two trained models (smiling, and non-smiling) used in "Testing GAN Models" experiment in Section 4.

This section describes the details of the two GAN models (smiling, and non-smiling models) we use in the "Testing GAN Models" experiment in Section 4. We use the CelebA dataset [Liu et al., 2015] in which each data point is an image of a celebrity with 40 binary attributes annotated e.g., pointy nose, smiling, mustache, etc. We create a partition of the images on the *smiling* attribute, thereby creating two disjoint subsets of *smiling* and *non-smiling* images. To reduce confounding factors that are not related to smiling (e.g., sunglasses, background), each image is cropped to be 64x64 pixels, so that only the face remains. Cropping and image alignment with eyes and lips are done with the software described in Amos et al. [2016]. We use DCGAN architecture [Radford et al., 2015] (for both generator and discriminator) for both smiling and non-smiling models, coded in Pytorch. Subsampling was performed so that the training sizes for the two models are equal. Each model is trained on 84,822 images (i.e., 84822 smiling faces, and 84822 non-smiling faces) for 50 epochs. The training time was roughly three hours using an Nvidia Titan X graphics card with Pascal architecture. We use Adam optimizer [Kingma and Ba, 2014] with $\beta_1 = 0.5$ and $\beta_2 = 0.999$. The learning rate is set to 10^{-3} (for both discriminator and generator in the two models). Some samples generated from the two trained models are shown in Figure 6.

⁴Code for FSSD released by the authors: <https://github.com/wittawatj/kernel-gof>.

C Proofs

This section contains proofs for the results given in the main text.

C.1 Proof of Theorem 1

Let all the notations be defined as in Section 3. Recall Theorem 1:

Theorem 1 (Asymptotic distribution of \widehat{S}_n^U). *Define $C_W^Q := \text{cov}_{\mathbf{y} \sim Q}[\psi_W(\mathbf{y}), \psi_W(\mathbf{y})]$, $C_V^P := \text{cov}_{\mathbf{x} \sim P}[\psi_V(\mathbf{x}), \psi_V(\mathbf{x})]$, and $C_{VW}^R := \text{cov}_{\mathbf{z} \sim R}[\psi_V(\mathbf{z}), \psi_W(\mathbf{z})] \in \mathbb{R}^{J_p \times J_q}$. Let $S^U := U_P^2 - U_Q^2$, and $M := \begin{pmatrix} \psi_V^P - \psi_V^R & \mathbf{0} \\ \mathbf{0} & \psi_W^Q - \psi_W^R \end{pmatrix} \in \mathbb{R}^{(J_p + J_q) \times 2}$. Assume that 1) P, Q and R are all distinct, 2) (k_X, V) are chosen such that $U_P^2 > 0$, and (k_Y, W) are chosen such that $U_Q^2 > 0$, 3) $\begin{pmatrix} \zeta_P^2 & \zeta_{PQ} \\ \zeta_{PQ} & \zeta_Q^2 \end{pmatrix} := M^\top \begin{pmatrix} C_V^P + C_V^R & C_{VW}^R \\ (C_{VW}^R)^\top & C_W^Q + C_W^R \end{pmatrix} M$ is positive definite. Then, $\sqrt{n}(\widehat{S}_n^U - S^U) \xrightarrow{d} \mathcal{N}(0, 4(\zeta_P^2 - 2\zeta_{PQ} + \zeta_Q^2))$*

Proof. Consider a random vector $\mathbf{t} := (\mathbf{x}, \mathbf{y}, \mathbf{z}) \in \mathcal{X}^3$, where \mathbf{x}, \mathbf{y} , and \mathbf{z} are independently drawn from P, Q , and R , respectively. Let T be the distribution of \mathbf{t} , and $\{\mathbf{t}_i\}_{i=1}^n = \{(\mathbf{x}_i, \mathbf{y}_i, \mathbf{z}_i)\}_{i=1}^n \stackrel{i.i.d.}{\sim} T$. Define two functions

$$\begin{aligned} \delta_V^P(\mathbf{t}, \mathbf{t}') &:= (\psi_V(\mathbf{x}) - \psi_V(\mathbf{z}))^\top (\psi_V(\mathbf{x}') - \psi_V(\mathbf{z}')), \\ \delta_W^Q(\mathbf{t}, \mathbf{t}') &:= (\psi_W(\mathbf{y}) - \psi_W(\mathbf{z}))^\top (\psi_W(\mathbf{y}') - \psi_W(\mathbf{z}')), \end{aligned}$$

where $\mathbf{t}' := (\mathbf{x}', \mathbf{y}', \mathbf{z}')$. It can be seen that $\delta_V^P(\mathbf{t}, \mathbf{t}') = \delta_V^P(\mathbf{t}', \mathbf{t})$ and $\delta_W^Q(\mathbf{t}, \mathbf{t}') = \delta_W^Q(\mathbf{t}', \mathbf{t})$ for all $\mathbf{t}, \mathbf{t}' \in \mathcal{X}^3$, and that both functions are valid U-statistic kernels. It is not difficult to see that \widehat{U}_P^2 and \widehat{U}_Q^2 (estimator given in Section 2) can be written in the form of second-order U-statistics [Serfling, 2009, Chapter 5] as

$$\begin{aligned} \widehat{U}_P^2 &= \binom{n}{2}^{-1} \sum_{i=1}^n \sum_{j < i} \delta_V^P(\mathbf{t}_i, \mathbf{t}_j), \\ \widehat{U}_Q^2 &= \binom{n}{2}^{-1} \sum_{i=1}^n \sum_{j < i} \delta_W^Q(\mathbf{t}_i, \mathbf{t}_j). \end{aligned}$$

Since $\psi_V^P \neq \psi_V^R$ (because $U_P^2 > 0$), \widehat{U}_P^2 is a non-degenerate U-statistic. Since $\psi_W^Q \neq \psi_W^R$, \widehat{U}_Q^2 is also non-degenerate [Serfling, 2009, Section 5.5.1]. By Hoeffding [1948, Theorem 7.1], asymptotically their joint distribution is given by a normal distribution:

$$\sqrt{n} \left(\begin{pmatrix} \widehat{U}_P^2 \\ \widehat{U}_Q^2 \end{pmatrix} - \begin{pmatrix} U_P^2 \\ U_Q^2 \end{pmatrix} \right) \xrightarrow{d} \mathcal{N} \left(\mathbf{0}, 4 \begin{pmatrix} \zeta_P^2 & \zeta_{PQ} \\ \zeta_{PQ} & \zeta_Q^2 \end{pmatrix} \right), \quad (1)$$

where

$$\begin{aligned} \zeta_P^2 &= \mathbb{V}_{\mathbf{t} \sim T} [\mathbb{E}_{\mathbf{t}' \sim T} [\delta_V^P(\mathbf{t}, \mathbf{t}')]] \stackrel{(a)}{=} (\psi_V^P - \psi_V^R)^\top (C_V^P + C_V^R) (\psi_V^P - \psi_V^R), \\ \zeta_Q^2 &= \mathbb{V}_{\mathbf{t} \sim T} [\mathbb{E}_{\mathbf{t}' \sim T} [\delta_W^Q(\mathbf{t}, \mathbf{t}')]] \stackrel{(b)}{=} (\psi_W^Q - \psi_W^R)^\top (C_W^Q + C_W^R) (\psi_W^Q - \psi_W^R), \\ \zeta_{PQ} &= \text{cov}_{\mathbf{t} \sim T} \left(\mathbb{E}_{\mathbf{t}' \sim T} [\delta_V^P(\mathbf{t}, \mathbf{t}')] , \mathbb{E}_{\mathbf{t}' \sim T} [\delta_W^Q(\mathbf{t}, \mathbf{t}')] \right) \stackrel{(c)}{=} (\psi_V^P - \psi_V^R)^\top C_{VW}^R (\psi_W^Q - \psi_W^R), \end{aligned}$$

and $C_{VW}^R := \text{cov}_{\mathbf{z} \sim R}[\psi_V(\mathbf{z}), \psi_W(\mathbf{z})] \in \mathbb{R}^{J_p \times J_q}$. At (a), (b), (c), we rely on the independence among \mathbf{x}, \mathbf{y} , and \mathbf{z} . A direct calculation gives the expressions of ζ_P^2 , ζ_Q^2 , and ζ_{PQ} . By the continuous mapping theorem, and (1), $\sqrt{n} \begin{pmatrix} 1 \\ -1 \end{pmatrix}^\top \left(\begin{pmatrix} \widehat{U}_P^2 \\ \widehat{U}_Q^2 \end{pmatrix} - \begin{pmatrix} U_P^2 \\ U_Q^2 \end{pmatrix} \right) = \sqrt{n}(\widehat{S}_n^U - S^U) \xrightarrow{d}$

$\mathcal{N} \left(\mathbf{0}, 4 \begin{pmatrix} 1 \\ -1 \end{pmatrix}^\top \begin{pmatrix} \zeta_P^2 & \zeta_{PQ} \\ \zeta_{PQ} & \zeta_Q^2 \end{pmatrix} \begin{pmatrix} 1 \\ -1 \end{pmatrix} \right)$ giving the result. \square

Table 2: Discriminator and generator of LSGAN used in experiment 5.

Discriminator	Generator
Input: 28×28 grayscale image	Input noise vector $z \sim \text{Unif}[0, 1]^{62}$
4×4 conv. 64 LReLU. Stride 2.	FC. 1024 RELU. Batch norm.
4×4 conv. 128 LReLU. Stride 2. Batch norm.	FC. $7 \times 7 \times 128$ RELU. Batch norm.
FC. 104 Leaky RELU. Batch norm.	4×4 upconv. 64 RELU. Stride 2. Batch norm.
FC	4×4 upconv. 1 channel.

conv. refers to a convolution layer, FC means a fully-connected layer, RELU means a rectified linear unit, LReLU means Leaky RELU, and upconv is the transposed convolution.

Remark 1. The assumption that P, Q , and R are all distinct in Theorem 1 is necessary for \widehat{U}_P^2 and \widehat{U}_Q^2 to follow a non-degenerate normal distribution asymptotically. If $R \in \{P, Q\}$, then \widehat{U}_S^2 for $S \in \{P, Q\}$ asymptotically follows a weighted sum of chi-squared random variables, and $U_S^2 = 0$. If $P = Q$, the covariance matrix in (1) is rank-deficient.

D Details of Experiment 5: Examining GAN Training

LSGAN Architecture We rely on Pytorch code⁵ by Hyeonwoo Kang to train the LSGAN [Mao et al., 2017] model that we use in experiment 5. Network architectures of the generator and the discriminator follow the design used in Chen et al. [2016, Section C.1]. We reproduce here in Table 2 for ease of reference.

Kernel Function The kernel k is chosen to be a Gaussian kernel on features extracted from a convolutional neural network (CNN) classifier trained to classify the ten digits of MNIST. Specifically the kernel k is $k(x, y) = \exp\left(-\frac{\|f(x) - f(y)\|_2^2}{2\nu^2}\right)$, where f is the output (in \mathbb{R}^{10}) of the last fully-connected layer of a trained CNN classifier.⁶ The architecture of the CNN is

Input: 28×28 grayscale image $\rightarrow 5 \times 5$ conv. 10 filters. 2×2 max pool
 $\rightarrow 5 \times 5$ conv. 20 filters. 2×2 max pool
 \rightarrow FC. 50 RELU.
 \rightarrow FC. 10 outputs.

We train the CNN for 30 epochs and achieve higher than 99% accuracy on MNIST’s test set. The Gaussian bandwidth ν is set with the median heuristic.

Class Proportion of Generated Digits To examine the proportion of digits in the generated samples, we sample 4000 images from both models P (LSGAN-15, LSGAN model trained for 15 epochs), and Q (LSGAN-17, LSGAN model trained for 17 epochs), and use the CNN classifier to assign a label to each image. The proportions of digits are shown in Figure 7. We observe that the generated digits from both LSGAN-15 and LSGAN-17 follow the right distribution i.e., uniform distribution, up to variability due to noise. There is no mode collapse problem. This observation means that the difference between P and Q studied in experiment 5 in the main text is not due to the mismatch of class proportions.

⁵<https://github.com/znxlwm/pytorch-generative-model-collections> (commit: 0d183bb5ea)

⁶Code to train the CNN classifier is taken from <https://github.com/pytorch/examples/blob/master/mnist/main.py> (commit: 75e7c75).

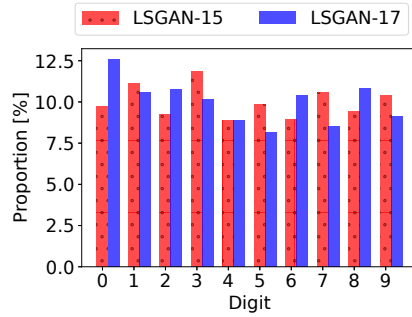
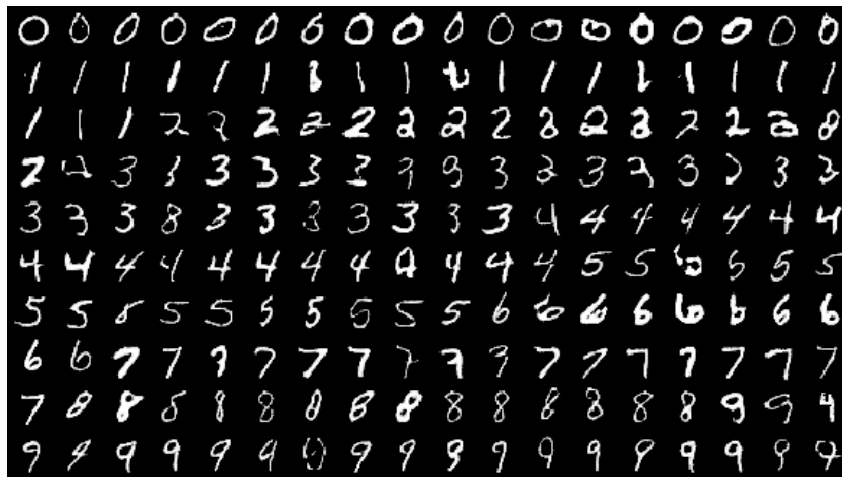
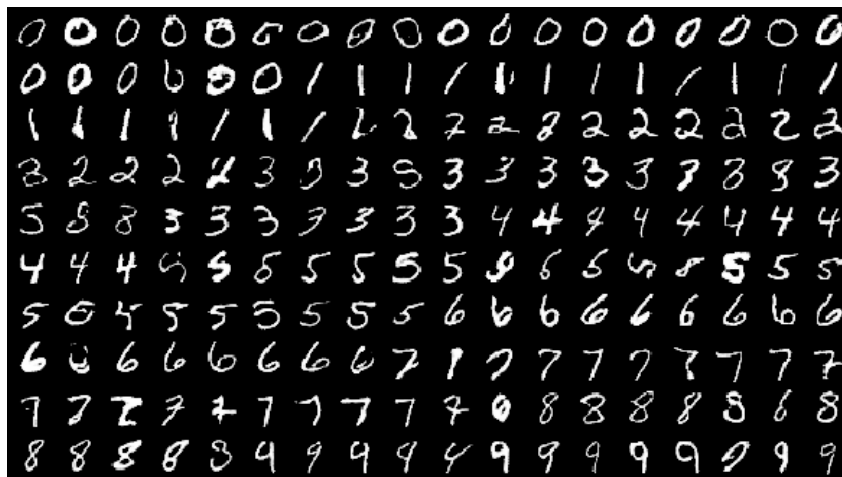


Figure 7: Proportions of generated digits from the LSGAN models at 15th and 17th epochs. Classification of each generated image is done by a trained convolutional neural network classifier (see Section D).



(a) Samples from LSGAN trained for 15 epochs.



(b) Samples from LSGAN trained for 17 epochs.

Figure 8: Samples from LSGAN models trained on MNIST. Samples are taken from the models at two different time points: after 15 epochs, and after 17 epochs of training.

E Comparing Different GAN Models Trained on MNIST

This section extends experiment 5 in the main text to compare other GAN variants trained on MNIST. All the GAN variants that we consider have the same network architecture as described in Table 2. We use the notation $AAA-n$ to refer to a GAN model of type AAA trained for n epochs. We note that the result presented here for each GAN variant does not represent its best achievable result.

WGAN-GP-10 vs LSGAN-10 Here we compare $P =$ Wasserstein GAN with Gradient Penalty [Gulrajani et al., 2017] and $Q =$ LSGAN [Mao et al., 2017] trained for ten epochs on MNIST. The results are shown in Figure 9. From the generated samples from the two models, it appears that LSGAN yields more realistic images of handwritten digits, after training for ten epochs. The positive power criterion values in Figure 9c further confirm this observation i.e., Q is better at all digits.

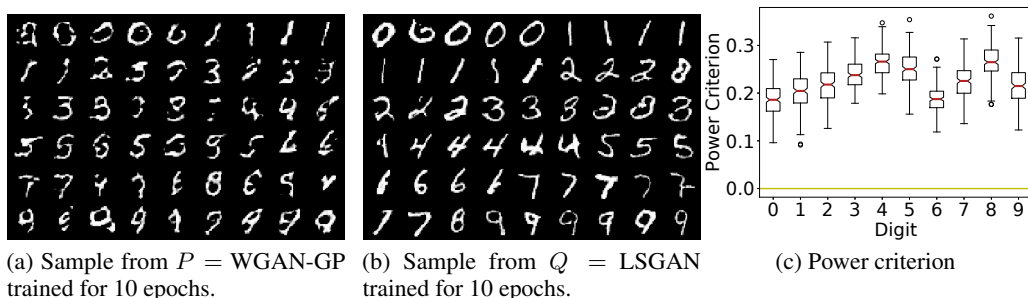


Figure 9: Comparing WGAN-GP (Wasserstein GAN with Gradient Penalty) and LSGAN, trained for ten epochs on MNIST.

GAN-40 vs LSGAN-40 In this part, we compare $P =$ GAN-40 [Goodfellow et al., 2014] and $Q =$ LSGAN trained for 40 epochs on MNIST. The results are shown in Figure 10. It can be seen from visual inspection that LSGAN-40 is slightly better overall, except for digits 1 and 5 at which LSGAN-40 appears to be significantly better. This observation is also hinted by the power criterion values at digits 1 and 5 which tend to be positive (see Figure 10c).

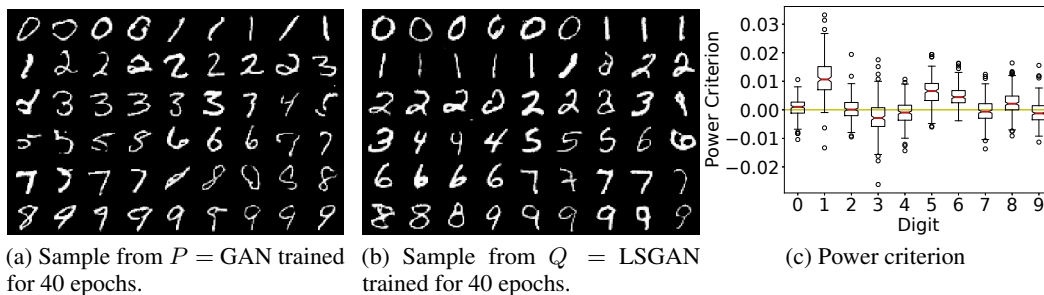
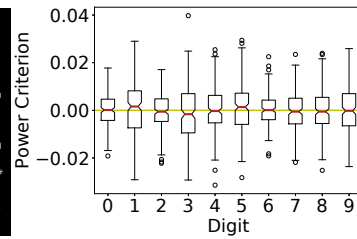


Figure 10: Comparing GAN (the original formulation) and LSGAN, trained for 40 epochs on MNIST.

WGAN-30 vs WGAN-30 As a sanity check, we also run the same procedure on a case where $P = Q$. We set $P = Q =$ Wasserstein GAN (WGAN, [Arjovsky et al., 2017] trained for 30 epochs on MNIST. The results are shown in Figure 11. As expected, the power criterion values spread around zero in all cases. We note that we did not modify the procedure to treat this special case. In particular, in each trial, two samples are drawn from P and Q as usual.



(a) Sample from $P = Q =$ WGAN trained for 30 epochs.



(b) Power criterion

Figure 11: Comparing two models which are the same for sanity checking. The model is set to WGAN trained for 30 epochs.